Multivariate quantification of landscape spatial heterogeneity using variogram models

Sébastien Garrigues, Denis Allard, Frédéric Baret, J. Morisette

HAL Id: hal-02669075
https://hal.inrae.fr/hal-02669075v1

Submitted on 31 May 2020

Multivariate Quantification of Landscape Spatial Heterogeneity using Variogram Models

Garrigues, S.[1], Allard, D.[2], Baret, F.[3], Morisette, J.[4]

[1]: University of Maryland's Earth System Science Interdisciplinary Center, College Park, MD

    Mailing address: NASA GSFC, Mail Code 614.4, Greenbelt MD, 20771

    Phone: 301 6146646

    Email address:Sebastien.garrigues@gsfc.nasa.gov

[2]: Biostatistic & Spatial Processes Unit, INRA, Avignon, France

[3]: UMR1114, INRA, Avignon, France

[4]: NASA's GSFC, Mail Code 614.5, Greenbelt, MD, USA

Submitted for Remote Sensing of Environment

Index terms: spatial heterogeneity, spatial structure, length scale, moderate spatial resolution, landscape, multivariate variogram model, red and near infrared reflectances, NDVI, stationarity.

Abstract

The monitoring of earth surface processes at a global scale requires high temporal frequency remote sensing observations provided up to now by moderate spatial resolution sensors (from 250 m to 7 km).

Non linear estimation processes of land surface variables derived from remote sensing data can be biased by the surface spatial heterogeneity within the moderate spatial resolution pixel. Quantifying this surface spatial heterogeneity is thus required to correct non linear estimation processes of land surface variables. The first step in this process is to properly characterize the scale of spatial variation of the processes structuring the landscape. Since the description of land surface processes generally involves various spectral bands, a multivariate approach to characterize the surface spatial heterogeneity from multi-spectral remote sensing observations has to be established.

This work aims at quantifying the landscape spatial heterogeneity captured by red and near infrared high spatial resolution images using direct and cross variograms modeled together with the geostatistical linear model of coregionalization. This model quantifies the overall spatial variability and correlation of red and near infrared reflectances over the scene. In addition, it provides an explicit understanding of the landscape spatial structures captured by red and near infrared reflectances and is thus appropriate to describe landscapes composed of areas with contrasted red and near infrared spectral properties.

The application of the linear model of coregionalization to 18 contrasted landscapes provides a spatial signature of red and near infrared spectral properties characterizing each type of landscape. Low vegetation cover sites are characterized by positive spatial correlation between red and near infrared. The mosaic pattern of vegetation fields and bare soil fields over crop sites generates high and negative spatial correlation between red and near infrared and increases the spatial variability of red and near infrared. On forest sites, the important amount of vegetation limits the spatial variability of red and the shadow effects mainly captured by near infrared induce a low and positive spatial correlation between red and near infrared.

Finally, the linear model of coregionalization applied to red and near infrared is shown to be more powerful than the univariate variogram modeling applied to NDVI because the second

order stationarity hypothesis on which variogram modeling relies is more frequently verified for red and near infrared than for NDVI.

1 Introduction

The monitoring of earth surface dynamic processes such as the exchanges of mass and energy between soil, vegetation and atmosphere requires observations of earth surface properties at the proper spatial and temporal scales. Remote sensing data are particularly appropriate to describe surface processes since they provide frequent spatial estimates of key earth surface variables (Sellers, 1997). To resolve rapid changes of vegetation status and amount under the influence of both climate and human activities, relatively high revisit frequency observations are required, currently provided by moderate resolution sensors with pixel size ranging from 250 m to 7 km (e.g. MODIS/TERRA-AQUA, MERIS/ENVISAT, VEGETATION/SPOT, POLDER/PARASOL). Since the landscape is a mosaic of objects, such as agricultural fields or vegetation patches, which are often smaller than moderate resolution pixels (Garrigues *et al.*, 2006a), the surface spatial heterogeneity information is lost at moderate spatial resolution. Characterizing the surface spatial heterogeneity is mandatory to identify the scale of spatial variation of surface processes structuring the landscape (Pielke and Avissar, 1990; Hipps and Neale, 1996; Wendroth *et al.*, 1999; Csillag and Kabos, 2002; Lyons and Halldin, 2004) and thus to improve their representation in land surface models (Schimel *et al.*, 1993; Pellenq *et al.*, 2003; Ahl *et al.*, 2004; Merlin *et al.*, 2005). In addition, intra-pixel spatial heterogeneity biases the estimation of land surface variable (e,g. Leaf Area Index, Land Surface Temperature, etc) from moderate resolution observations when the algorithm relating land surface variable and radiometric data is non linear (Raffy, 1994; Friedl *et al.*, 1995; Hu and Islam, 1997; Heuvelink and Pebesma, 1999; Lovejoy *et al.*, 2001; Garrigues *et al.*, 2006b). To limit its influence on the description of land surface processes, a first approach consists in explicitly taking into account the intra-pixel spatial heterogeneity in non linear retrieval algorithm (Garrigues *et al.*, 2006b). A second approach is to use the surface spatial heterogeneity information to disaggregate moderate spatial resolution estimates of land surface variables at their proper scale of spatial variation (Faivre and Fischer, 1997; Pellenq *et al.*, 2003; Merlin *et al.*, 2005;). Both strategies require quantifying the surface spatial heterogeneity from high spatial resolution observations (with pixel size ranging from 10 m to 30 m). Since, most land surface variables are estimated using more than one spectral band, multivariate approaches to characterize the surface spatial heterogeneity from multi-spectral remote sensing observations have to be developed.

Garrigues *et al.*, 2006a provide detailed definitions of the spatial heterogeneity measured from remote sensing sensors as well as the factors (Sampling step and Point Spread Function of the sensor, scene extent, *etc.*) influencing its characterization. We highlight here the main points of these definitions. Spatial heterogeneity of a given surface property is described through two components:

- The spatial variability of the surface property over the observed scene (*i.e.* variance of the remote sensing image).

- The spatial structures: they are defined as patches or objects (e.g. agricultural fields, forest stands, vegetation patches, *etc.*) that repeat themselves independently within the observed scene at a characteristic length scale (*i.e.* spatial scale) which represents the extent of the spatial structure. They can be viewed as the typical correlation area (*i.e.* the typical area of influence) of the surface property. Spatial structures within remotely sensed images are identifiable in that their spectral properties are more homogeneous within them than between them and other scene elements (Jupp *et al.*, 1988). Data are often distributed into independent sets of spatial structures, related to different length scales and spatial variability, being overlaid in the same region.

In this work, red and near infrared reflectances are the state variables used to describe the spatial heterogeneity of the vegetation cover at the landscape level defined here as an area of few square kilometers (9 to 50 km^2). The spatial heterogeneity is quantified from high spatial resolution data (e.g. SPOT-HRV, nominal pixel size of 20m) that have been shown to be fine enough to resolve the spatial structures of most landscapes and coarse enough to limit the noise generated by spatial structures at very small length scales that may hamper the proper characterization of the spatial structures of vegetation cover at the landscape level (Garrigues *et al.*, 2006a). Spatial variability within high spatial resolution pixels is mainly generated by spatial structures within the canopy. It will not be considered here because this paper specifically focuses on the quantification of the spatial heterogeneity at the landscape level. However, the methodology presented here can easily be extended to quantify the spatial heterogeneity at the canopy level using very high spatial resolution data (with pixel size smaller than 5m).

Garrigues *et al.*, 2006a provide a comparison of some second order statistics tools relevant to describe the spatial variations within an image. Among these tools, the variogram has been widely used to understand the nature and the causes of spatial variation within an image (Woodcock *et al.*, 1988a) such as radiometric contrast between the image objects (Curran, 1988; Woodcock *et al.*, 1988a; Woodcock *et al.*, 1988b; St-Onge and Cavayas, 1995;

Bruniquel-Pinel and Gastellu-Etchegorry, 1998), the mean size of the image objects (Woodcock *et al.*, 1988a; Woodcock *et al.*, 1988b; Lacaze *et al.*, 1994) or the multiscale spatial structuring of the image (Lacaze *et al.*, 1994; Oliver, 2001). Besides, Garrigues *et al.*, 2006a demonstrated that modeling the variogram of high spatial resolution NDVI (Normalized Difference Vegetation Index derived from red and near infrared reflectances) image is an efficient method to quantify the spatial heterogeneity components (spatial variability and spatial structure) of the landscape.

The surface spatial heterogeneity is strongly dependent on the radiometric variable used to characterize it (Curran, 1988; Chavez, 1992; Lacaze *et al.*, 1994; Atkinson, 1999). Garrigues *et al.*, 2006a demonstrated that the NDVI variogram is efficient to characterize the influence of the land use on the landscape spatial heterogeneity. However, the NDVI variogram may be limited to capture some landscape pattern such as the spatial structures within a soil area which are better described by red reflectances (Lacaze et al., 1994). Therefore, variograms from multiple spectral bands such as red and near infrared may provide additional information compared to NDVI variogram to better understand the processes structuring the landscape.

In addition, Garrigues *et al.*, 2006b proposed to use the variogram of high spatial resolution radiometric data as a proxy for the spatial heterogeneity within moderate resolution pixel covering the same area as the high spatial resolution image in order to correct the scaling bias associated with non linear estimation of land surface variables over heterogeneous pixels. Since most land surface variable retrieval algorithms capitalizes on more than one spectral band or single vegetation index (Weiss and Baret 1999), multivariate variogram modeling, as developed in this work, is required to quantify the mean variability of each spectral band and co-variability between spectral bands within the moderate resolution pixel and implement Garrigues *et al.*, 2006b 's approach.

Most studies investigating the dependency between spatial heterogeneity and radiometric variables were limited to comparing experimental variograms computed over simulated landscape images or over a limited number of land cover types. The first objective of this paper is to extend the univariate variogram modeling developed by Garrigues et al, 2006a to multivariate variogram modeling. This will allow for explicit quantification of the spatial heterogeneity captured by two spectral bands; here red and near infrared high spatial resolution images, over various types of landscape. This approach will prove to be powerful to assess the spatial variability and co-variability of red and near infrared reflectances for three generic types of landscape, namely sparse natural vegetation; cropland and grassland; forest. The second objective of this paper is to show that multivariate variogram modeling

applied to red and near infrared reflectances provides a more comprehensive characterization of the landscape spatial structures than NDVI variogram modeling.

In the Second Section, the 18 contrasted landscapes extracted from the VALERI (Validation of Land European Remote sensing Instruments) database and used in this study, are described along with the SPOT-HRV scenes used to describe the surface spatial heterogeneity. The third section is dedicated to the bivariate variogram modeling methodology applied to red and near infrared high spatial resolution images. In Section four, the parameters of the bivariate variogram models are used to quantify the spatial heterogeneity captured by red and near infrared over different types of landscape. Finally, in Section five, the "stationarity" of the data required to properly characterize the landscape spatial structures by the variogram is discussed for the red, near infrared and NDVI variables.

2 Data description

The data used here are part of the VALERI database (Baret *et al.*, accepted), which provides SPOT-HRV scenes at 20m spatial resolution for multiple landscapes sampled through the world. For this study, 18 contrasted spatial heterogeneity sites were selected (Table 1). Each site has the following characteristics: 3 km by 3 km size, relatively flat topography, and contains one or two types of vegetation including crop, grass, needleleaf forest, broadleaf forest or shrubland. Note that for this study only 3km by 3km subset of the SPOT-HRV scenes was available over each site of the VALERI database.

The reflectance was measured in three spectral bands: green (0.5-0.59μm), red (0.61-0.67μm), near infrared (0.78-0.89μm). In this paper, the red (denoted *r(x)*, where *x* represents a pixel of the SPOT-HRV image) and near infrared (denoted *p(x)*) reflectances are the 'state variables' used to describe the spatial heterogeneity of the landscape. The Normalized Difference Vegetation Index (NDVI) derived from these reflectances (Jackson, 1983),

$$NDVI(x) = \frac{p(x) - r(x)}{p(x) + r(x)}$$

(1)

will be used in Section 5 to evaluate the potential of NDVI variograms to characterize the spatial structures of the landscapes compared to red and near infared variograms.

The SPOT-HRV scenes are georeferenced in the UTM/WGS84 projection. They are not contaminated by clouds except in the tropical forest image (Counami01) for which a cloud mask was applied. They are not corrected for atmospheric scattering and absorption. But, for most scenes, the atmospheric effects are low in the red and near-infrared bands and their spatial variability is small over 3 km by 3 km scenes (Baret *et al.*, accepted).

3 Bivariate variogram modeling

As pointed out by Garrigues *et al.*, 2006a, the characterization of landscape spatial heterogeneity from the selected SPOT-HRV scenes requires several assumptions.

- A_1: the image extent (3000m) is large with respect to the spatial features of interest. This assumption is verified for most sites because the size of their typical objects is much lower than the site extent, and there is no obvious gradient through the images.

- A_2: the radiometric measurement errors (cloud detection, atmospheric effects, resampling effects, …) are assumed to be small relative to the surface variations. This assumption is acceptable because the selected images are cloud-free, and the homogeneity of sensor calibration and atmospheric correction is relatively even over such limited extent areas.

- A_3: Effect of spatial variations at scale smaller than the sampling step of the sensor (20 m) can be neglected. This is based on the fact that the combination of the Point Spread Function and the sampling step of the sensor are such that effects of spatial variations within a 20 m pixel are very small relative to the environmental variations.

- A_4: coregistration errors between the SPOT-HRV spectral bands are small enough to assume that the spatial supports of red and near infrared data are identical.

Bivariate variogram modeling approach follows two steps. The experimental variogram of red and near infrared reflectances and the experimental cross variogram between these variables are first computed at the image scale. Variograms and cross variograms are then modeled together using the widely used linear coregionalization model (Wackernagel, 2003).

3.1 Experimental direct and cross variograms

Red and near infrared reflectances are considered as values of punctual regionalized variables (Matheron, 1965) *r(x)* and *p(x)*, respectively, describing the spatial distribution of the landscape vegetation cover over the image domain, *I*.

The experimental direct variograms associated with *r(x)*,

$$\gamma_{e,r}(h) = \frac{1}{2N(h)} \sum_{\|x_\alpha - x_\beta\| \approx h} \left(r(x_\alpha) - r(x_\beta)\right)^2 ,$$

(2)

and *p(x)*,

$$\gamma_{e,p}(h) = \frac{1}{2N(h)} \sum_{\|x_\alpha - x_\beta\| \approx h} \left(p(x_\alpha) - p(x_\beta)\right)^2 ,$$

(3)

measure the average of squared differences between reflectance values of all the pair of pixels *(x_α, x_β)* separated by a vector *h*. The experimental cross variogram between *p(x)* and *r(x)*,

$$\gamma_{e,p,r}(h) = \frac{1}{2N(h)} \sum_{\|x_\alpha - x_\beta\| \approx h} \left(p(x_\alpha) - p(x_\beta)\right)\left(r(x_\alpha) - r(x_\beta)\right)$$

(4)

describes the spatial co-variability between the variables *p(x)* and *r(x)* over the scene. In Equation 2, 3 and 4, *N(h)* represents the number of paired pixels separated by a vector *h*.

Experimental direct and cross variograms can be computed for a specific direction (*h* is then a vector) or without specifying a direction (*h* is reduced to a distance). In this work, the spatial distributions of the red and near infrared reflectances are assumed to be isotropic and the experimental direct and cross variograms are computed by pooling together all directions. This assumption is not absolutely necessary. However, since isotropy is verified for most of the 18 images analyzed in this paper, we introduce it for the clarity of exposition. The methodology presented below can easily be extended to the case of non isotropic variogram models.

Variogram values are not statistically reliable at large distances (Chilès and Delfiner, 1999). We therefore decided to compute the variogram up to the maximum distance d_{max}=1500m equal to half the extent of the images, as advised by these authors.

Experimental direct and cross variograms are characterized by several key properties (Chilès and Delfiner, 1999). Direct variogram is usually an increasing function of the distance $||h||$ (Figure 1) since values of pixels close together are likely to be more similar than values of pixels far apart. The cross variogram is related to the spatial distribution of the correlation between the variables $p(x)$ and $r(x)$. It is an increasing function of the distance $||h||$ when $p(x)$ and $r(x)$ are positively correlated (Figure 1.c) and it is a decreasing function of the distance $||h||$ when $p(x)$ and $r(x)$ are negatively correlated (Figure 1.d). It may also display both negative and positive spatial correlation characterizing two different sets of spatial structures associated with distinct spectral red and near infrared properties (Figure 1.b: $\gamma_{e,p,r}(h)$ decreases first and then increases at large distance).

At large distance, direct and cross variograms may reach a sill or increase indefinitely. Most experimental variograms of the images under study reach a sill before d_{max}. This indicates that most images are large enough to encompass the spatial variability of the landscape spatial structures and confirms the acceptability of assumption A_1. The sill of the direct variograms of $p(x)$ and $r(x)$ quantifies the overall spatial variability of $p(x)$ and $r(x)$, respectively. The sill of the cross-variogram between $p(x)$ and $r(x)$ quantifies the overall covariance between $p(x)$ and $r(x)$. For few images, the sill is not reached before d_{max} indicating that the image is not large enough to encompass the low frequency variation in the data (Chilès and Delfiner, 1999; Garrigues *et al.*, 2006a). This is due to spatial structures extending beyond the image extent creating apparent trends in the image. A criterion will be given in Section 3.2.3 to judge if the image size is large enough to encompass the spatial variability of the landscape spatial structures.

The variogram ranges are characteristic distances at which variograms reach their sill (or 95% of the sill for exponential variogram, see Section 3.2). They are related to the length scales (*i.e.* spatial scale) of the data. A variogram may display several ranges characterizing the multiscale spatial structuring of the data.

The behavior of the variogram near the origin is an important property of the variogram which reflects the continuity of the variable under study. In particular, a discontinuity of the variogram at the origin, also called nugget effect, can be related to either uncorrelated noise (measurement error) or to spatial structures at a length scale smaller than the pixel size. All experimental variograms computed on the VALERI images are linear at the origin, without any apparent nugget effect. This observation is a strong support to the assumptions (A_2) and (A_3).

3.2 Linear coregionalization model

3.2.1 Theoretical direct and cross-variograms.

A probabilistic model for the regionalized variables *p(x)* and *r(x)* is used to quantify the landscape spatial heterogeneity captured by red and near infrared high spatial resolution images

In the framework of second order stationary random functions (Chilès and Delfiner, 1999; Wackernagel, 2003), *p(x)* and *r(x)* are regarded as one among all possible realizations of the (second order stationary) random functions *P(x)* and *R(x)*, respectively. Second order stationarity of *P(x)* and *R(x)* assumes the existence and the stationarity of the first and second moments,

$$E[P(x)] = m_p, \quad E[R(x)] = m_r, \quad Cov(P(x), P(x+h)) = C_p(h), \quad Cov(R(x), R(x+h)) = C_r(h)$$

(5)

$$Cov(P(x), R(x+h)) = C_{p,r}(h), \qquad Cov(R(x), P(x+h)) = C_{r,p}(h),$$

(6)

for all *x* and *h*. The functions $C_p(h)$ and $C_r(h)$ are the covariance functions characterizing *P(x)* and *R(x)*, respectively, while $C_{p,r}(h)$ and $C_{r,p}(h)$ are the cross-covariance functions. Note that $C_{p,r}(h) \neq C_{p,r}(-h)$, but that $C_{p,r}(h) = C_{r,p}(-h)$. Under second order stationarity assumption, the theoretical direct variograms associated with *P(x)*

$$\gamma_p(h) = 0.5 Var[P(x+h) - P(x)],$$

(7)

and *R(x)*,

$$\gamma_r(h) = 0.5 Var[R(x+h) - R(x)],$$

(8)

are related to the covariance functions according to the relationships,

$$\gamma_p(h) = \sigma_p^2 - C_p(h)$$

(9)

and

$$\gamma_r(h) = \sigma_r{}^2 - C_r(h) \, ,$$

(10)

where $\sigma_p{}^2$ and $\sigma_r{}^2$ are the theoretical variances of *P(x)* and *R(x)*, respectively. The theoretical variogram is a function starting from 0 for $||h||$=0 and ultimately converging to the sill as $||h||$ tends to infinity. The range of the theoretical variogram is the distance at which it reaches a sill (or 95% of the sill for exponential variogram). Data separated by a distance larger than the range are uncorrelated (or very weakly correlated with a correlation less than 0.05 for exponential model).

The theoretical cross variogram associated to the vector of second order stationary random functions (*P(x)*, *R(x)*) is defined by:

$$\gamma_{p,r}(h) = 0.5E\big[(P(x+h) - P(x))(R(x+h) - R(x))\big]$$

(11)

It can be shown that $\gamma_{p,r}(h) = 0.5\,(C_{p,r}(h) + C_{p,r}(-h))$. The cross variogram corresponds thus to the even part of the covariance function $C_{p,r}(h)$. It is bounded by the direct variograms of *P(x)* and *R(x)* (Wackernagel, 2003):

$$-\sqrt{\gamma_p(h)\gamma_r(h)} \le \gamma_{p,r}(h) \le \sqrt{\gamma_p(h)\gamma_r(h)}$$

(12)

The comparison of the cross variogram with respect to its lower and upper bounds characterizes the spatial distribution of the correlation between red and near infrared reflectances over the scene (Figure 1). When the cross variogram is close to its upper bound, *i.e.* the ratio $\dfrac{\gamma_{p,r}(h)}{\sqrt{\gamma_p(h)\gamma_r(h)}}$ is close to 1, red and near infrared reflectances are highly positively correlated. When the cross variogram is close to its lower bound, *i.e.* the ratio $\dfrac{\gamma_{p,r}(h)}{\sqrt{\gamma_p(h)\gamma_r(h)}}$ is close to -1, red and near infrared reflectances are highly negatively correlated (Figure 1.d).

The theoretical direct and cross variograms are estimated by fitting a valid mathematical function to the experimental direct and cross variograms (Chilès and Delfiner, 1999). These functions, also called authorized models, must be conditionally negative functions (Wackernagel, 2003). Exponential and spherical functions are used in this work since they

suit the main properties of the experimental direct and cross variograms: linear behavior and continuity at the origin; convergence to a sill. Table 2 provides the characteristics of those two variogram functions. Note that the range parameter of the exponential function is the so called practical range, *i.e.* the distance at which the variogram reaches 95% of the sill.

3.2.2 Linear model of coregionalization

In this paper, direct and cross variograms are modeled together using the widely used linear model of coregionalization (Wackernagel, 2003). This model is the multivariate extension of the linear model of regionalization used by Garrigues *et al.*, 2006a to model the NDVI variogram. In this model, theoretical direct and cross variograms are weighted sums of the same *l* elementary variogram functions (here exponential or spherical functions with unit sill), $g_k(a_k, h)$, $k=1, ..., l$:

$$\gamma_p(h) = \sigma_p^2 \sum_{k=1}^{k=l} b_k^p g_k(a_k, h)$$

(13)

$$\gamma_r(h) = \sigma_r^2 \sum_{k=1}^{k=l} b_k^r g_k(a_k, h)$$

(14)

$$\gamma_{p,r}(h) = \sigma_{p,r}^2 \sum_{k=1}^{k=l} b_k^{p,r} g_k(a_k, h)$$

(15)

This model is particularly appropriate to describe independent sets of spatial structures, being overlaid in the same scene, related to different length scales and red and near infrared spatial variability and co-variability. It quantifies the landscape spatial heterogeneity captured by red and near infrared through the following components:

- *overall spatial variability and co-variability over the scene:* the direct variogram sills σ_p^2 and σ_r^2 quantify the overall image variance of red and near infrared, respectively. The cross variogram sill $\sigma_{p,r}^2$ represents the overall spatial covariance between red and near infrared. The theoretical correlation coefficient,

$$\rho_{p,r} = \frac{\sigma_{p,r}^2}{\sqrt{\sigma_p^2 \sigma_r^2}} \; ,$$

(16)

is an indicator of the overall spatial correlation between red and near infrared over the scene.

- *Image spatial structures:* Each image spatial structure modeled by the linear model of coregionalization is characterized by the following parameters:

  - The ranges a_k associated with the elementary functions g_k characterize the length scales of the scene.

  - The variance weights b_k^p and b_k^r quantify the fractions of the overall variance of near infrared and red images, respectively, for each structure k. Similar variance weights b_k^p and b_k^r show that near infrared and red variables vary over the same set of spatial structures, *i.e.* they capture the same spatial structures within the landscape, and vice versa.

  - The correlation coefficient,

$$\rho_k^{p,r} = \frac{\sigma_{p,r}^2 b_k^{p,r}}{\sqrt{\sigma_p^2 b_k^p \sigma_r^2 b_k^r}} = \rho_{p,r} \frac{b_k^{p,r}}{\sqrt{b_k^p b_k^r}} \; ,$$

(17)

quantifies the spatial correlation between red and near infrared associated with the structure k.

The parameters of the linear coregionalization model are estimated by a semi-automatic fitting method (Isatis software, http://www.geovariances.com). First, the number of necessary elementary variograms, l, and the associated ranges are visually adjusted. Here, it is always found sufficient to have l equal to one or two. Then, the sill and the variance weights are estimated by weighted mean square optimization under the linear coregionalization model constraints. We refer to Goulard and Voltz, 1992; Morisette, 1997; Wackernagel, 2003 for a complete description of the method. The linear coregionalization model is valid only if all coregionalization matrices,

$$B_k^{p,r} = \begin{matrix} b_k^p & b_k^{p,r} \\ b_k^{p,r} & b_k^r \end{matrix}$$

(18)

associated with each structure $k=1,...,l$, are semi-definite positive which implies that each elementary function $g_k(a_k,h)$ part of the cross variogram is also part of the direct variograms. In this sudy, both direct and cross variograms are defined by the same elementary functions $g_k(a_k,h)$.

Since experimental direct and cross variograms are not trustworthy for distances larger than d_{max}, any estimated variogram range above this distance is deemed not reliable and therefore was not considered. In this case, the underlying second order stationarity hypothesis must be rejected. Note that among the 18 sites under study, only 4 sites have an estimated range larger than d_{max} (Table 3).

3.2.3 Quantification of the image spatial structures

The integral range A (Equation 19) summarizes all structural parameters of the direct variogram model $\gamma(h)$ (ranges a_k and fraction of total variance b_k) into a single characteristic area (Serra, 1982; Chilès and Delfiner, 1999; Garrigues *et al.*, 2006a).

$$A = \frac{1}{\sigma^2} \int_{h \in \Re^2} \left(\sigma^2 - \gamma(h) \right) dh$$

(19)

For the linear model of coregionalization, the integral range is computed for each direct variogram $\gamma_p(h)$ and $\gamma_r(h)$. It is the weighted linear combination of the integral range A_k of each elementary variogram functions $g_k(a_k,h)$. The integral ranges of red and near infrared variograms are given by Equation 20 and 21, respectively.

$$A_r = \sum_{k=1}^{l} b_k^r A_k,$$

(20)

$$A_p = \sum_{k=1}^{l} b_k^p A_k,$$

(21)

with

$$A_k = \int_{h \in \Re^2} \left(1 - g_k(a_k, h)\right) dh$$

(22)

Table 2 gives the value of A_k for the spherical and exponential models (Lantuéjoul, 2002).

As shown in Garrigues *et al.*, 2006a, the square root D_c of the integral range which is a weighted average of the several range parameters of the variogram model quantifies the mean length scale of the data, *i.e.* the mean extent of the image spatial structures captured by the data. Therefore, the parameters D_c of red (denoted D_c^r) and near infrared (denoted D_c^p) quantify the mean extent of the spatial structures resolved by red and near infrared, respectively. Different value of D_c^r and D_c^p indicates that red and near infrared capture different spatial structures in the landscape.

The integral range of a given variable can also be used as a yardstick to judge if the size of the image of that variable is large enough to encompass the spatial variability of the spatial structures captured by that variable and thus if the second order stationarity hypothesis on which the modeling of the variogram relies is consistent with the data. Garrigues *et al.*, 2006a propose that the integral range must be smaller than 5% of the image surface, *i.e.* D_c, must thus be smaller than $D_{c,T,3km}$ =671m for a 3000m by 3000m image. This criterion will be used in Section 5 to discuss the "stationarity" of red and near infrared compared to that of NDVI. The parameters D_c of NDVI variogram (denoted D_c^{NDVI}) are provided by Garrigues et al, 2006a for the same sites presented here.

4 Results

4.1 Overall spatial variability and correlation of red and near infrared

Near infrared and red reflectances are sensitive to the amount of vegetation covering the surface (Myneni and Ross, 1991; Price, 1996). Generally, near infrared reflectance increases over vegetation area because leaves are more reflective than soil and the multiple scattering within the canopy increases the signal measured by the sensor. Red reflectance is low over vegetation area (absorption by chlorophyll) and increases over low vegetation cover and bare soil area. In the following, the amount of vegetation will be quantified by the Leaf Area Index (LAI) variable defined as half the total developed area of leaves per unit ground horizontal surface area (Chen and Black, 1992). As the LAI increases, the reflectance decreases in the

red and increases in the near infrared (Sellers, 1987; Myneni and Ross, 1991; Price, 1996). However, the non linear relationship between reflectance and LAI induces the saturation of the radiometric signal (Myneni *et al.*, 2002): near infrared saturates for LAI larger than 6-8 while red saturates for LAI larger than 3-4 (when the vegetation cover of the surface is complete, *i.e.* no soil effect).

Given these properties, one can distinguish three major types of landscape with distinct red and near infrared spectral signatures (Figure 2). In this section, we will use the parameters of the linear model of coregionalization applied to the SPOT-HRV scenes under study (Figure 5, Table 3) to quantify for each type of landscape (Figure 2) the overall spatial variability of red (σ_r^2) and near infrared (σ_p^2), as well as the overall spatial correlation ($\rho_{p,r}$) between red and near infrared.

4.1.1 Sparse natural vegetation sites (low vegetation cover)

On Turco02 and Gourma00, the vegetation cover is low (low LAI) which induces an important soil effect on the radiometric signal. Since red and near infrared have similar spectral signature over soil (along the soil line on Figure 2), the overall correlation between red and near infrared reflectances is high and positive over these sites (0.88 for Turco02 and 0.95 for Gourma00). Since the soil properties and the vegetation cover are homogeneous over these sites, the overall spatial variability of red and near infrared are low.

4.1.2 Crop and grassland sites (medium vegetation cover)

Crop sites are globally characterized by high overall spatial variability of near infrared (σ_p^2) and red (σ_r^2) compared to other types of landscape, as well as high and negative overall spatial correlation $\rho_{p,r}$ between red and near infrared. This is due to their mosaic spatial structure of bare soil and low vegetation cover fields with increasing red reflectances and decreasing near infrared reflectances and crop fields with decreasing red reflectances and increasing near infrared reflectances. The overall spatial variability σ_p^2 of near infrared is mainly explained by the differences of near infrared values between fields caused by the nature and state of the crops. The overall spatial variability σ_r^2 of red reflectances is lower than that of near infrared σ_p^2 because the differences of reflectance values between vegetation and bare soil fields are lower in the red than in the near infrared. But it is generally higher over crop sites than over most natural vegetation and forest sites since crop sites contain bare soil area alternating with vegetation area. It is particularly high on Barrax03 due to the variations of soil properties

(texture, presence of vegetation regrowth…) within the large bare soil area covering this site (Figure 3).

On Barrax03 and Gilching02, the magnitude of the correlation $\rho_{p,r}$ is low compared to other crop sites. This is due to the presence of a contrasting area (forest on Gilching02, Figure 4 and large bare soil area on Barrax03, Figure 3) over which red and near infrared are positively correlated, thus compensating for the negative correlation associated with the field spatial structures. This analysis will be refined by the characterization of the spatial structures of these sites in Section 4.2.2.

On grassland (Larzac02 and Laprida01), the important vegetation cover saturating the signal in the red explains the low spatial variability of red. On Larzac02, the homogeneity of LAI over the scene explains the very low spatial variability of near infrared. On Laprida01 the variations of LAI due to grazing activity increases the overall spatial variability of near infrared. The overall correlation of grassland sites is negative but its magnitude is lower than on crop sites that is probably due to the saturation of red reflectances.

4.1.3 Forest sites (high vegetation cover)

Over forest, the important amount of vegetation which includes green understorey, high density of trees and the presence of broad leaves saturates the signal in the red (saturation for LAI larger than 3), causing to limit the red spatial variability. Near infrared reflectance captures some variations of LAI. However, the LAI variability is too small over the forest sites under study to explain the whole spatial variability of near infrared. In addition, near infrared also tends to saturate for LAI larger than 6. The main source of spatial variability of the radiometric signal is the shadow effects caused by variations of canopy architecture, density of trees and size of the crowns. These shadow effects are mainly captured by near infrared reflectances characterized by an overall spatial variability close to that of crop sites (for Jarvselja01, mixed forest σ_p^2 =0.0045 and for SudOuest02, crop σ_p^2=0.0046). However, they are poorly resolved by red reflectances (low overall spatial variability) because the red radiometric resolution is not fine enough to detect the very low variations of red reflectances generated by the shadow effects. Since shadows affect both red and near infrared in the same way, the overall spatial correlation $\rho_{p,r}$ is generally positive over forest. However, because of the limitation of the red radiometric resolution, the magnitude of the spatial correlation is low over most forest sites.

Some forest sites are not in agreement with these findings. On Counami01 and Aekloba01, sites characterized by a very dense vegetation cover (LAI larger than 6), the shadow effects

are limited and the radiometric signal saturates, thus explaining the very low spatial variability of near infrared over these sites. On other sites, the presence of spatial structures with contrasting red reflectances (young seedling plantation, bare soil and water area on Concepcion03 and Hirsikangas03; quarry and rocky area on Puechabon01) increases the overall spatial variability of red. The very low overall correlation between red and near infrared (close to zero) observed on some sites is caused by various factors such as the presence of water (e.g. Larose03) which affects the radiometric signal. In contrast, on Puechabon01, the presence of rocky area and a quarry associated with both increasing values of red and near infrared increases the magnitude of the overall correlation over this forest site.

4.2 Image spatial structures

On some sites the overall correlation is low with regard to the type of vegetation (e.g Barrax03 and Gilching02). The parameters (σ_p^2, σ_r^2, $\rho_{p,r}$) are not always sufficient to understand the nature and the causes of the spatial variations over the scene. In this section, we analyze the structural parameters of the coregionalization model in order to understand the differences in spatial structures captured by red and near infrared reflectances over the scene. In the first sub-section, we globally quantify these differences by comparing the mean extent of the spatial structures captured by red (D_c^r) and near infrared (D_c^p) for the 18 landscapes under study. In the second sub-section, we use all the structural parameters of the linear model of coregionalization to characterize the nature and the scale of variation of each spatial structure captured by red and near infrared over two particular sites.

4.3.1 Overall quantification of the spatial structures captured by red and near infrared.

Figure 6 displays the comparison of D_c^r and D_c^p. On most crop sites (except Gilching02 and Barrax03), D_c^r and D_c^p are similar. This indicates that red and near infrared capture the same mosaic spatial structure of agricultural fields that explains the high magnitude of the spatial correlation between red and near infrared over crop sites. The differences between D_c^r and D_c^p observed on Gilching02 and Barrax03 are explained in the following sub-section.

On most forest sites (e.g. Jarvselja01, Larose03), red and near infrared generally do not capture the same spatial structures (D_c^r and D_c^p are different) which explains the low magnitude of the spatial correlation between red and near infrared over forest sites. D_c^p characterizes the mean extent of the spatial structures generated by both the variations of LAI

and the variations of canopy structure (shadow effects). The early saturation and radiometric resolution of the red band limit the detection of these spatial structures by red which explains the lower value of D_c^r than D_c^p observed on most forest sites. On the Counami01 tropical forest site, both red and near infrared saturates, which explains their low degree of structuring (low and similar values of D_c^r and D_c^p,).

4.3.2 Characterization of near infrared and red spatial variability and correlation at the spatial structure scale

Among the 18 sites under study, Gilching02 and Barrax03 present a feature that deserves a specific mention. They are composed of two spatial structures with very contrasting red and near infrared spectral properties (Figure 3 and Figure 4). As a result, red and near infrared do not capture the same spatial structures over these sites (as shown by the differences between D_c^r and D_c^p) and their overall correlation is low compared to other crop sites. We chose to analyze these two particular sites to illustrate the potential of the coregionalization model to discriminate spatial structures with distinct red and near infrared spectral properties. For this, we use the structural parameters (b_k^p, b_k^r, $\rho_k^{p,r}$) of the linear model of coregionalization (Table 3) which quantify the spatial variability and correlation of red and near infrared associated with each spatial structure *k*.

Gilching02 is composed of a forest area and a crop area (Figure 4). The first structure of the linear model of coregionalization (Figure 1.b, Table 3) is characterized by a negative correlation coefficient ($\rho_1^{p,r}$ = −0.48) and an associated short range (*a₁=380m*). It explains most of the near infrared overall spatial variability ($b_1^p = 93\%$) and a significant part of the red overall spatial variability ($b_1^r = 40\%$). It is related to a large extent to the mosaic spatial structure of agricultural fields captured by both red and near infrared. But it is also influenced by the variations of LAI and canopy structure (shadow effects) within the forest area which are detected by near infrared (Figure 4). The forest spatial structure (Figure 1.b, Table 3) is associated with a larger range *a₂=1180m* and is characterized by a positive correlation coefficient ($\rho_2^{p,r}$ = 0.99). It is mainly captured by red reflectances ($b_2^r = 60\%$) which are more homogeneous within the forest area than between the forest area and other scene elements (Figure 4).

On Barrax03, irrigation discs of vegetation are laid over a large bare soil background (Figure 3). The positive correlation coefficient associated with the first structure (Figure 1.a, Table 3) characterizes the small bare soil fields ($a_1=400m$) within the bare soil area. The variation in soil properties is mainly captured by red reflectances ($b_1^r = 61\%$). This is also detected by near infrared but generating a lower spatial variability of near infrared ($b_1^p = 7.5\%$) than that of red. The second structure (Figure 1.a, Table 3) is related to the irrigation discs of vegetation with a range value similar to the average extent of the discs ($a_2=800m$). The spatial structure of the vegetation discs is mainly captured by near infrared ($b_2^p = 93\%$) because of the high variability of near infrared between vegetation discs and bare soil fields. The spatial structure of vegetation disc also explains $b_2^r = 39\%$ of the overall variability of red which are more homogeneous within the vegetation fields than between them and other scene elements. In agreement with other crop sites, the alternation of bare soil and vegetation fields generates a negative correlation associated with the second spatial structure of the linear model of coregionalization.

Garrigues *et al.*, 2006a show that NDVI variogram of Barrax03 detects only the vegetation disc spatial structures and did not describe the spatial structures within the bare soil area. Besides, the information provided by the NDVI variogram of Gilching02 was not sufficient to clearly identify the two spatial structures composing the scene. As stated in Section 3, the linear model of coregionalization is appropriate to describe independent sets of spatial structures being overlaid in the same scene. It is not a hierarchical model for two stage systems such as forest area and a finer scale of variation within the forest as it is the case for Gilching02 (Figure 4). But despite this fact, the linear model of coregionalization applied to red and near infrared on Gilching02 is able to provide a more comprehensive characterization of the nature of the processes structuring this hierarchical landscape than NDVI variogram modeling.

5 Discussion: Stationarity of red and near infrared variables

In the previous sections, we used bivariate variogram models applied to red and near infrared to characterize the landscape spatial heterogeneity. Garrigues et al., 2006a performed the same analysis for the univariate variogram modeling applied to NDVI which combines red and near infrared variables in one synthetic variable. To demonstrate the utility of the bivariate variogram modeling, we propose here to evaluate the "stationarity" of red and near

infrared variables compared to that of NDVI (Equation 1). Indeed, variogram modeling relies on the second order stationarity hypothesis which ensures that the variogram characterizes properly the landscape spatial structures. To verify if the second order stationarity hypothesis of a given variable is consistent with the data, *i.e.* the image extent of that variable is large enough to encompass the spatial variability of the spatial structures captured by that variable, we use the criterion defined in Section 3.2.3 stating that the mean length scale D_c of the variable must be smaller than the threshold $D_{c,T,3km}=671\ m$ for a 3km image.

Figure 7 displays a comparison of D_c^r, D_c^p and D_c^{NDVI}. The values of D_c^{NDVI} are provided by Garrigues et al., 2006a for the same scenes under study. On most crop sites, D_c^r, D_c^p and D_c^{NDVI} show similar values smaller than $D_{c,T,3km}$ indicating that red, near infrared and NDVI capture the same mosaic pattern of agricultural fields which is completely characterized at the image scale. On forest and natural vegetation sites, the image extent is not always large enough to resolve the spatial variability of the landscape spatial structures. This is due to spatial structures extending beyond the image extent or to the presence of a contrasting spatial structure in the border of the image (Garrigues et al., 2006a). For example, on Concepcion03, the presence of a large area of young seedling plantation (characterized by the second range r_2=1800 m) in the border of the scene explains the non stationarity of red, near infrared and NDVI (D_c^r, D_c^p and D_c^{NDVI} larger than $D_{c,T,3km}$). The non stationarity can affect the three variables red, near infrared and NDVI or only one particular variable. Figure 7 shows that the non stationarity of NDVI is more frequent than that of red and near infrared. Indeed, on Puechabon01, Nezer01 and Hirsikangas03 D_c^{NDVI} is larger than $D_{c,T,3km}$ while D_c^r and D_c^p are smaller than $D_{c,T,3km}$.

Since the second order stationarity hypothesis is verified on more sites for red and near infrared than for NDVI, bivariate variogram modeling applied to red and near infrared appears to be more powerful than NDVI variogram modeling to characterize the spatial structures of the landscapes under study.

Conclusions

This work highlights the potential of multi-spectral remote sensing observations to quantify the landscape spatial heterogeneity. It shows that direct and cross variograms modeled together using the linear coregionalization model are powerful tools to quantify the landscape spatial heterogeneity captured by red and near infrared high spatial resolution images. The linear model of coregionalization quantifies the overall spatial variability and correlation of red and near infrared over the scene. In addition, it provides an explicit understanding of the landscape spatial structures captured by red and near infrared over the scene that it is particularly appropriate to describe landscapes composed of areas with contrasted red and near infrared spectral properties. Each spatial structure is characterized by i) the spatial variability and correlation of red and near infrared explained by the spatial structure and by ii) the variogram range which is an indicator of the extent of the spatial structure. The integral range which summarizes all structural parameters of the variogram into a single characteristic area is computed for each red and near infrared direct variogram. Its square root quantifies the mean extent of the image spatial structures captured by red and near infrared. It is also used to judge if the size of the scene is large enough to encompass the spatial variability of the landscape spatial structures captured by each variable and thus if the second order stationarity hypothesis on which the modeling of the variograms relies is consistent with the data.

The application of the linear model of coregionalization to 18 contrasted landscapes provides a spatial signature of red and near infrared spectral properties characterizing each type of landscape. Low vegetation cover sites are characterized by a high positive spatial correlation between red and near infrared due to the soil effect on the radiometric signal. On crop sites, the mosaic pattern of bare soil fields and crop fields is captured by both red and near infrared. As a result, red and near infrared are generally more variable over crop sites than over forest and natural vegetation sites and the spatial correlation between red and near infrared is generally high and negative. On forest sites, the important amount of vegetation homogenizes the spatial distribution of red except when the site contains low vegetation cover objects which increase the spatial variability of red. The shadow effects caused by the variations of the forest canopy structure are the main sources of spatial variability on the radiometric signal, generating positive spatial correlation between red and near infrared. However, while shadow effects are captured by near infrared, their detection by red is limited by the red

radiometric resolution that substantially decreases the magnitude of the spatial correlation between red and near infrared over forest sites.

Compared to NDVI variogram model, the linear model of coregionalization applied to red and near infrared provides a more comprehensive characterization of the spatial scale of variation and the nature of the processes structuring the landscapes on the 18 sites of the VALERI database. In addition, the second order stationarity hypothesis on which variogram modeling relies is more frequently verified for red and near infrared than for NDVI. As a result, bivariate variogram modeling applied to red and near infrared potentially has a broader range of application than NDVI variogram modeling in order to properly characterize the spatial structures of the landscapes under study.

However, the results of this paper are limited by the number, the type, the low complexity and the small size of the landscapes analyzed. In particular, for few landscapes, the 3000 m by 3000 m image size used in this work was too small to encompass the spatial variability of the landscape spatial structures. Additional works should thus consider larger area and a more representative sampling of landscape type in terms of different types of vegetation, land use, topography features and soil properties. Further studies should also apply the linear model of coregionalization to additional spectral bands or combination of spectral bands in order to capture other surface properties such as the vegetation water content described by middle infrared spectral band.

Finally, multivariate variogram model of high spatial resolution data can be used as a proxy for the spatial heterogeneity within moderate resolution pixel to correct the scaling bias associated with non linear estimation of land surface variables from multi-spectral observations over heterogeneous pixels (Garrigues *et al.*, 2006b). However, to implement this method, ways have to be found to get prior knowledge of variograms and cross-variograms of high spatial resolution data without systematic concurrent high spatial resolution images that would make moderate spatial resolution images useless. Ongoing works are investigating the possibility of using a temporal sampling of high spatial resolution multi-spectral data to retrieve the spatial heterogeneity within moderate resolution pixels and account for it in non linear retrieval algorithm of land surface variables.

Acknowledgements

References

Ahl, D.E., Gower, S.T., Mackay, D.S., Burrows, S.N., Norman, J.M. and Diak, G.R. (2004), Heterogeneity of light use efficiency in a northern Wisconsin forest: implications for modeling net primary production with remote sensing. *Remote Sensing of Environment,* 93, 168-178.

Atkinson, P.A. (1999), Exploring the relation between spatial structure and wavelength: implications for sampling reflectance in the field. *International Journal of Remote Sensing,* 20, 2663-2678.

Baret, F., Weiss, M., Allard, D., Garrigues, S., Leroy, M., Jeanjean, H., Fernandes, R., Myneni, R.B., Morissette, J.T., Privette, J., Bohbot, H., Bosseno, R., Dedieu, G., Di Bella, C., Espana, M., Gond, V., Gu, X.F., Guyon, D., Lelong, C., Maisongrande, P., Mougin, E., Nilson, T., Veroustraete, F. and Vintilla, R. (accepted), VALERI: a network of sites and a methodology for the validation of medium spatial resolution land satellite product. *Remote Sensing of Environment*.

Bruniquel-Pinel, V. and Gastellu-Etchegorry, J.-P. (1998), Sensitivity of texture of high resolution images of forest to biophysical and acquisition parameters. *Remote Sensing of Environment,* 65, 61-85.

Chavez, P.S. (1992), Comparison of spatial variability in visible and near infrared spectral images. *Photogrametry Engineering Remote Sensing,* 58, 957-964.

Chen, J.M. and Black, T.A. (1992), Defining leaf area index for non-flat leaves. *Plant Cell Environment,* 15, 421-429.

Chilès, J.-P. and Delfiner, P. (1999), *Geostatistics: Modeling Spatial Uncertainy*. New-York: Wiley Inter-Science, (695 p).

Csillag, F. and Kabos, S. (2002), Wavelets, boundaries and the analysis of landscape pattern. *Ecoscience,* 9(2), 177-190.

Curran, P.J. (1988), The semivariogram in remote sensing: an introduction. *Remote Sensing of Environment,* 24, 493-507.

Faivre, R. and Fischer, A. (1997), Predicting crop reflectances using satellite data observing mixed pixels. *Journal of Agricultural, Biological, and Environment Statistics,* 2(1), 87-107.

Friedl, M.A., Davis F.W., Michaelsen, J. and Moritz, M.A. (1995), Scaling and uncertainty in the relationship between the NDVI and land surface biophysical variables: An analysis using scene simulation model and data from FIFE. *Remote Sensing of Environment,* 54, 233-246.

Garrigues, S., Allard, D. and Baret , F. (2006b), Influence of the spatial heterogeneity on the non linear estimation of Leaf Area Index from moderate resolution remote sensing data. *Remote Sensing of Environment.,* 106, 286–298.

Garrigues, S., Allard, D., Baret , F. and Weiss, M. (2006a), Quantifying spatial heterogeneity at the landscape scale using variogram models. *Remote Sensing of Environment,* 103, 81-96.

Goulard and Voltz (1992), Linear coregionalization model: Tools for estimation and choice of cross-variogram matrix. *Mathematical Geology,* 24, 269-286.

Heuvelink, G.B.M. and Pebesma, E.J. (1999), Spatial aggregation and soil process modelling. *Geoderma,* 89, 47-65.

Hipps, D.O. and Neale, C.M.U. (1996), Spatial structure and scaling of surface fluxes in a Great Basin ecosystem. In Stewart, J. B., Engman, E. T., Feddes, R. A. and Kerr, Y., Eds., *Scaling up in Hydrology Using Remote Sensing* (pp. 113-124). Chichester, UK: Wiley.

Hu, Z. and Islam, S. (1997), A framework for analyzing and designing scale invariant remote sensing algorithms. *IEEE Transactions on Geoscience and Remote Sensing,* 35, 747-755.

Jackson, R.D. (1983), Spectral indices in n-space. *Remote Sensing of Environment,* 13, 409-421.

Jupp, D.L.B., Strahler, A.H. and Woodcock, C.E. (1988), Autocorrelation and regularization in digital images I: Basic Theory. *IEEE Transactions on Geoscience and Remote Sensing,* 26(4), 463-473.

Lacaze, B., Rambal, S. and Winkel, T. (1994), Identifying spatial patterns of Mediterranean landscapes from geostatistical analysis of remotely-sensed data. *International Journal of Remote Sensing,* 15(12), 2437-2450.

Lantuéjoul, C. (2002), *Geostatistical Simulation: Models and Algorithms*. Berlin: Springer Verlag, (256 p).

Lovejoy, S., Schertzer, D., Tessier, Y. and Gaonac'h, H. (2001), Multifractals and resolution-independent remote sensing algorithms: the example of ocean colour. *International Journal of Remote Sensing,* 22(7), 1191-1234.

Lyons, T.J. and Halldin, S. (2004), Surface heterogeneity and the spatial variation of fluxes. *Agricultural and Forest Meteorology,* 121(3-4), 153-165.

Matheron, G. (1965), *Les variables régionalisées et leur estimation*. Paris: Masson, (305 p).

Merlin, O., Chehbouni, G., Kerr, Y., Njoku, E. and Entekhabi, D. (2005), A combined modeling and multi-spectral/multi-resolution remote sensing approach for disaggregation of surface soil moisture: application to SMOS configuration. *IEEE Transactions on Geoscience and Remote Sensing,* 43, 2036-2050.

Morisette, J. (1997), Examples using SAS to fit the model of linear coregionalization. *Computer and Geosciences,* 23(3), 317-323.

Myneni, R.B., Hoffman, S., Knyazikhin, Y., Privette, J.L., Glassy, J., Tian, Y., Wang, Y., Song, X., Zhang, Y., Smith, G.R., Lotsch, A., Friedl, M., Morisette, J.T., Votava, P., Nemani, R.R. and Running, S.W. (2002), Global products of vegetation leaf area and fraction absorbed PAR from one year of MODIS data. *Remote Sens Environ,* 83, 214-231.

Myneni, R.B. and Ross, J. (1991), *Photon-vegetation interactions. Applications in optical remote sensing and plant ecology.* New York: Springer Verlag, (565 p).

Oliver, M.A. (2001), Spatial scale variation in environmental properties. In Tate, N. J. and Atkinson, P. M., Eds., *Modelling Scale in Geographic Information Science* (pp. 193-219). New York: Wiley.

Pellenq, J., Kalma, J., Boulet, G., Saulnier G.-M. , Wooldridge, S., Kerr, Y. and Chehbouni, A. (2003), A disaggregation scheme for soil moisture based on topography and soil depth *Journal of Hydrology,* 276, 112-123.

Pielke, R.A. and Avissar, R. (1990), Influence of landscape structure on local and regional climate. *Landscape Eclogy,* 4, 133-155.

Price, J.C., Steven, M.D., Andrieu, B. and Jaggard, K., (1996), Visible near-infrared radiation parameters for sugar beets. *International Journal of remote sensing,* 17(17), 3411-3418.

Raffy, A.M. (1994), Heterogeneity and change of scale in models of remote sensing- spatialization of multi-spectral models. *International Journal of Remote Sensing,* 15, 2359-2380.

Schimel, D.S., Davis, F.W. and Kittel, T.G.F. (1993), Spatial information for extrapolation of canopy processes: Examples from FIFE. In Ehleringer, J. R. and Field, C. B., Eds., *Scaling Physiological Processes. Leaf to Globe* (pp. 21-29). New-York: Academic Press.

Sellers, P.J. (1987), Canopy reflectance, photosynthesis and transpiration II. The role of biophysics in the linearity of their interdependence. *Remote Sensing of Environment,* 21, 143-183.

Sellers, P.J. (1997), Modeling the exchange of energy, water, and carbon between continents and atmosphere. *Science,* 275, 602-609.

Serra, J. (1982), *Image analysis and mathematical morphology*. London, New-York: Academic Press, (600 p).

St-Onge, B.A. and Cavayas, F. (1995), Estimating forest stand structure from high-resolution imagery using the directional variogram. *International Journal of Remote Sensing,* 16(11), 1999-2001.

Wackernagel, H. (2003), *Multivariate Geostatistics: An Introduction with Applications*. Berlin: Springer (387 p).

Weiss, M. and Baret , F. (1999), Evaluation of canopy biophysical variable retrieval performances from the accumulation of large swath satellite data. *Remote Sensing of Environment,* 70, 293-306.

Wendroth, O., Pohl, W., Koszinski, S., Rogasik, H., Ritsem, C.J. and Nielsen, D.R. (1999), Spatio-temporal patterns and covariance structures of soil water status in two Northeast-German field sites. *Journal of Hydrology,* 215, 38-58.

Woodcock, C.E., Strahler, A.H. and Jupp, D.L.B. (1988a), The use of variograms in remote sensing: a/ scene models and simulated images. *Remote Sensing of Environment,* 25, 323-348.

Woodcock, C.E., Strahler, A.H. and Jupp, D.L.B. (1988b), The use of variograms in remote sensing: b/ Real digital images. *Remote Sensing of Environment,* 25, 349-379.

Tables:

Table 1: Data base (detailed information on each site is available on the VALERI web site www.avignon.inra.fr/valeri). Date is the acquisition month of the image. m_{NDVI} and σ_{NDVI} are the mean and standard deviation of the NDVI image characterizing the mean and variability of vegetation amount over each site.

Landscape type	Site name	Site number	Biome	Date	Lat	Lon	m_{NDVI}	σ_{NDVI}
Crop and grassland	Fundulea01	1	Cropland	May	44.41	26.58	0.51	0.23
	Alpilles01	2	Cropland	Mar	43.81	4.74	0.41	0.19
	Barrax03	3	Cropland	Jul	39.06	2.10	0.29	0.19
	SudOuest02	4	Cropland	Jul	43.51	1.24	0.50	0.17
	Alpilles02	5	Cropland	Jul	43.81	4.74	0.38	0.16
	Gilching02	6	Cropland and mixed forest	Jul	48.08	11.33	0.60	0.12
	Laprida01	7	Grassland	Nov	36.99	-60.55	0.62	0.09
	Larzac01	8	Grassland	Jul	43.95	3.12	0.49	0.06
Forest	Larose03	9	Mixed forest	Aug	45.38	-75.22	0.70	0.06
	Jarvselja01	10	Mixed forest	Jul	58.29	27.29	0.82	0.05
	Hirsikangas03	11	Needleleaf forest	Aug	62.64	27.01	0.59	0.09
	Nezer01	12	Needleleaf forest (pine forest)	Jun	44.51	-1.04	0.66	0.06
	Concepcion03	13	Needleleaf forest (80% of pine)	Jan	-37.47	-73.47	0.69	0.09
	Aekloba01	14	Broadleaf forest (Palmtree plantation)	Jun	2.63	99.68	0.65	0.04
	Counami01	15	Broadleaf forest (tropical forest)	Oct	05.35	53.25	0.69	0.03
	Puechabon01	16	Closed shrubland (Mediterranean vegetation)	Jun	43.72	3.65	0.54	0.10
Sparse vegetation	Gourma00	17	Savanna	Sep	15.32	-1.55	0.22	0.01
	Turco02	18	Barren and sparse vegetation	Aug	-18.23	-68.18	0.11	0.01

Table 2: Characteristics of the spherical and exponential variogram models.

| Model	Formula ($\gamma(h)$)	Integral range (A)
Spherical (Sph)	$\gamma(h) = \begin{cases} \sigma^2\left(\dfrac{3}{2}\dfrac{h}{a} - \dfrac{1}{2}\left(\dfrac{h}{a}\right)^3\right) & \text{if } h \le a \\ \sigma^2 \text{ if } h > a \end{cases}$	$\dfrac{\pi a^2}{5}$
Exponential (Exp)	$\gamma(h) = \sigma^2\left(1 - \exp\left(-\dfrac{3h}{a}\right)\right)$	$\dfrac{2\pi a^2}{9}$

The term *h* represents the distance. In the spherical model, *a* is the variogram range (i.e. the distance at which the variogram reaches the sill σ^2) while in the exponential variogram *a* is the practical range (i.e. the distance at which the variogram reaches 95% of the sill σ^2).

Table3: Parameters of the linear model of coregionalization adjusted for each each site.

Landscape type	Site number	Overall spatial variability and correlation			First spatial structure				Second spatial structure				Mean length scales		
		σ_p^2	σ_r^2	$\rho_{p,r}$	$g_1(r_1)$	b_1^p	b_1^r	$\rho_1^{p,r}$	$g_2(r_2)$	b_2^p	b_2^r	$\rho_2^{p,r}$	D_c^p	D_c^r	D_c^{NDVI}
Crop and grassland	1	0.0148	0.00029	-0.91	$Sph(790)$	100	100	-0.91	/	0	0	0.00	626	626	619
	2	0.0048	0.00115	-0.68	$Sph(260)$	62.4	67.6	-0.56	$Sph(1290)$	37.6	32.4	-0.89	648	606	664
	3	0.0058	0.00615	-0.19	$Sph(400)$	7.5	61.1	0.62	$Sph(800)$	92.5	38.9	-0.54	616	467	514
	4	0.0046	0.00083	-0.66	$Sph(340)$	55.3	58.4	-0.40	$Sph(830)$	44.7	41.6	-0.99	484	472	513
	5	0.0030	0.00101	-0.55	$Sph(185)$	36.7	31.3	-0.35	$Sph(415)$	63.3	68.7	-0.65	276	285	289
	6	0.0064	0.00068	-0.05	$Exp(380)$	93.5	32.4	-0.48	$Sph(1180)$	6.5	67.6	0.99	389	790	493
	7	0.0031	0.00010	-0.27	$Exp(216)$	59.3	73	-0.18	$Sph(950)$	40.7	27	-0.44	500	421	562
	8	0.0007	0.00009	-0.35	$Exp(280)$	79.2	65	-0.55	$Sph(1400)$	20.8	35	0.17	548	683	506
forest	9	0.0025	0.00002	-0.10	$Exp(140)$	72.9	99.7	-0.08	$Sph(650)$	27.1	0.3	-0.99	286	120	236
	10	0.0045	0.00006	0.30	$Exp(194)$	69.8	90	0.33	$Sph(1078)$	30.2	10	0.23	489	311	550
	11	0.0034	0.00048	-0.01	$Exp(200)$	75.8	69.5	0.26	$Sph(1000)$	24.2	30.5	-0.76	416	459	1058
	12	0.0024	0.00018	0.26	$Exp(220)$	48.4	52	0.06	$Sph(750)$	51.6	48	0.46	446	433	922
	13	0.0032	0.00032	-0.04	$Exp(150)$	62.2	6.4	-0.31	$Sph(1800)$	37.8	93.6	0.03	930	1455	1014
	14	0.0002	0.00005	-0.15	$Exp(150)$	61.3	91	-0.06	$Sph(1800)$	38.7	9	-0.54	893	445	561
	15	0.0008	0.00001	0.43	$Exp(60)$	86.2	83.2	0.44	$Sph(700)$	13.8	16.8	0.35	211	232	215
	16	0.0010	0.00120	0.64	$Exp(350)$	39.7	59.6	0.77	$Sph(1000)$	60.3	40.4	0.53	674	577	841
Sparse vegetation	17	0.0007	0.00030	0.95	$Exp(70)$	10	22.2	0.89	$Sph(2000)$	90	77.8	0.97	1504	1399	1059
	18	0.0001	0.00010	0.88	$Exp(255)$	77.7	69.7	0.91	$Sph(2000)$	22.3	30.3	0.82	771	891	1053

The subscript r and p stands for red and near infrared, respectively. In the three first column, σ_r^2 and σ_p^2 measure the overall spatial variability of red and near infrared, respectively, over the scene and $\rho_{p,r}$ quantifies the overall spatial correlation between red and near infrared over the scene. Each image spatial structure k ($k=1,2$) is described by: 1) the elementary variogram model g_k (g_k is either an exponential *(Exp)* or spherical *(Sph)* model) function of the range a_k (in meter); 2) the fractions (in %) of the overall spatial variability of red b_k^r and near infrared b_k^p explained by the structure k; 3) the spatial correlation $\rho_k^{p,r}$ between red and near infrared generated by the structure k. D_c^r and D_c^p (in meter) are the mean length scale of red and near infrared, respectively. We added the mean length scale of the NDVI D_c^{NDVI} (provided by Garrigues et al, 2006a) for comparison purpose.
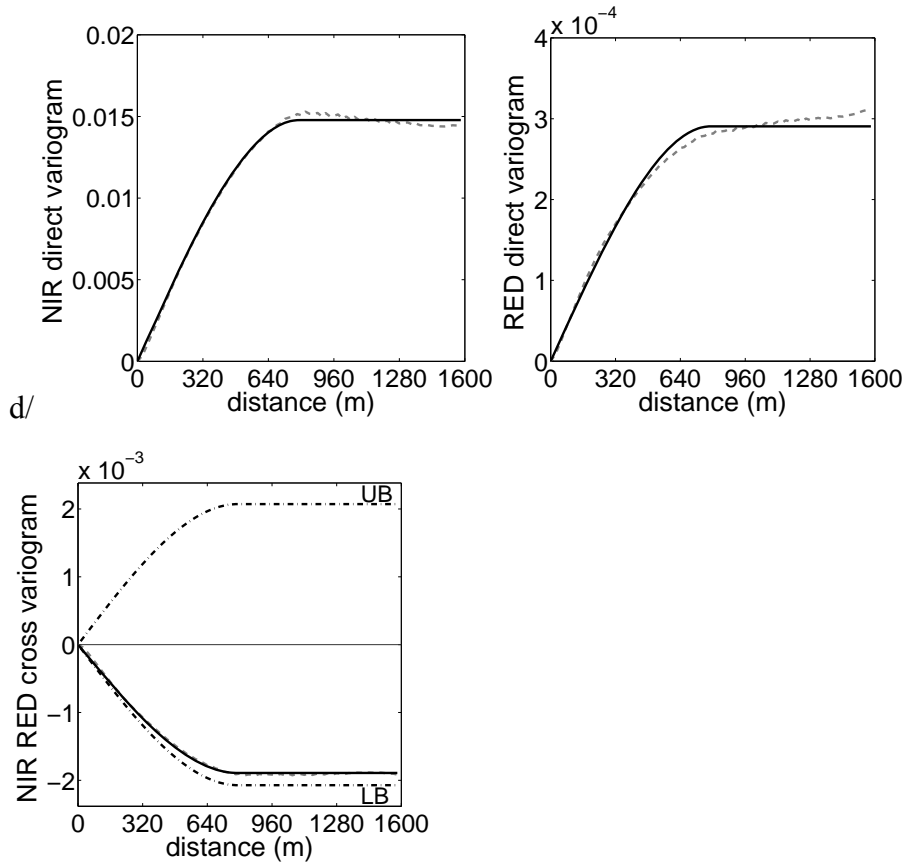
<u>Figures:</u>

a/

b/

c/
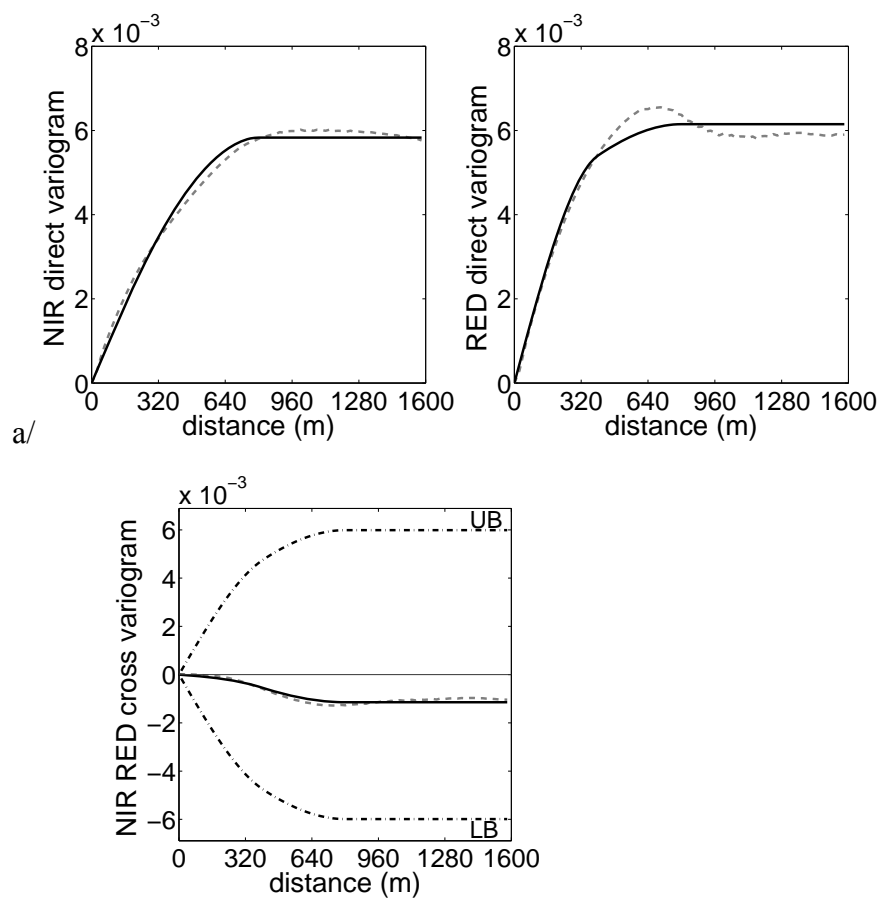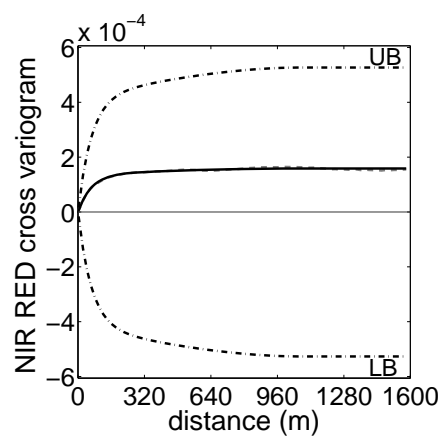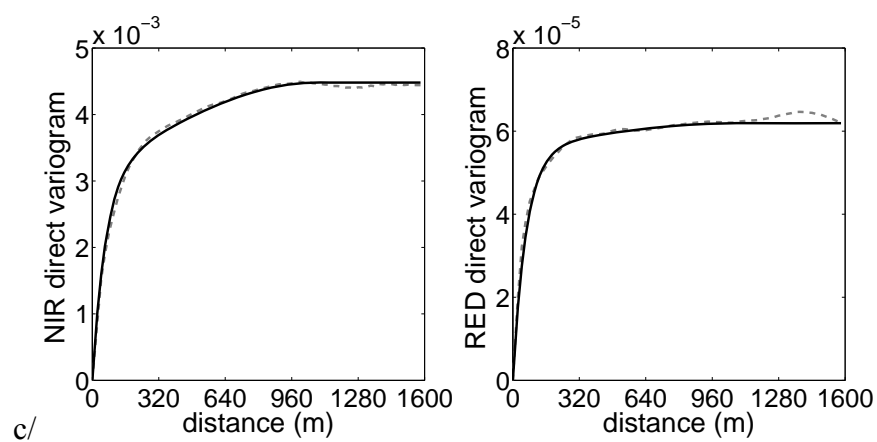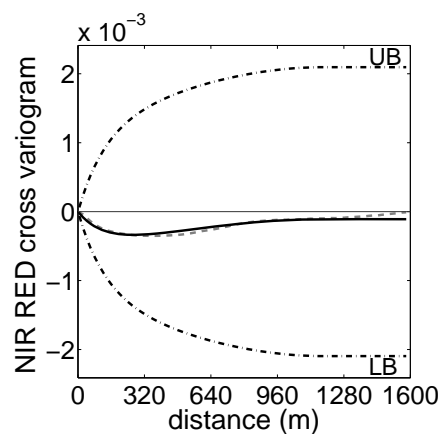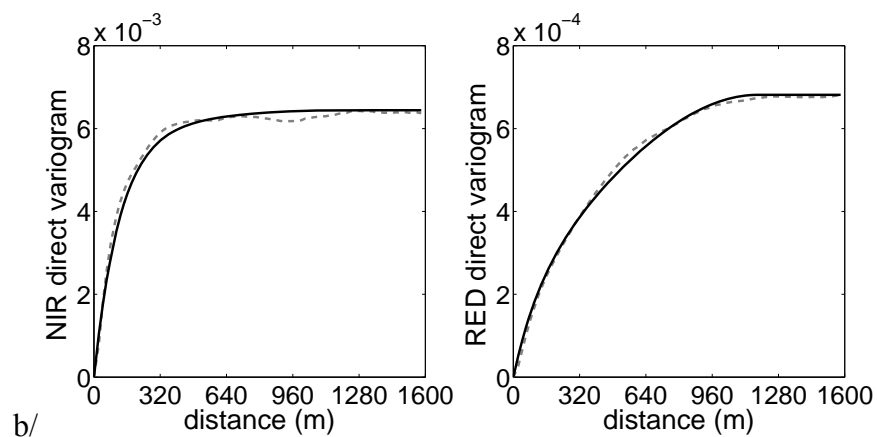
Figure 1: Direct and cross variograms of red (RED) and near infrared (NIR) for the following sites a/Barrax03, b/Gilching02, c/Jarvselja01, d/Fundulea01. The gray dashed lines (--) are the experimental variograms. The black solid lines represent the fitted variogram models. On the Figure of the NIR RED cross variogram the black dash-dot lines (-.-) represent the lower ($LB = -\sqrt{\gamma_p(h)\gamma_r(h)}$) and the upper ($UB = \sqrt{\gamma_p(h)\gamma_r(h)}$) bounds of the cross variogram model. The parameters of the variogram models are given in Table 3.
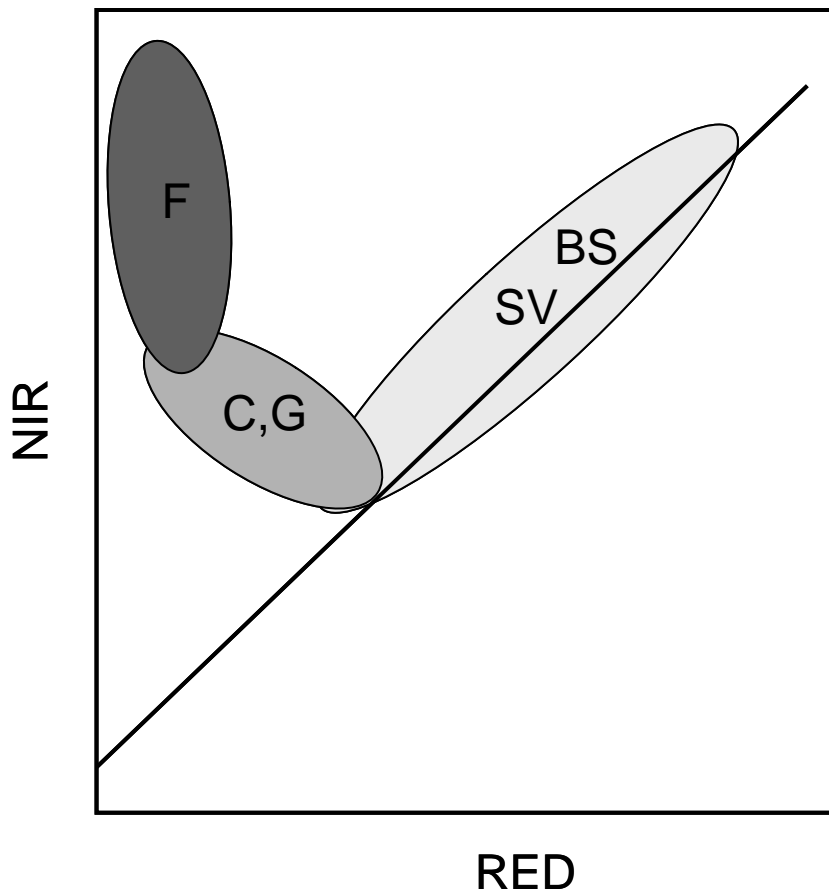
Figure 2: Red (RED) and near infrared (NIR) spectral signature of three types of landscape: forest (F); crop (C) and grassland (G); bare soil (BS) and sparse vegetation (SV). The solid line represents the soil line.

a/

b/
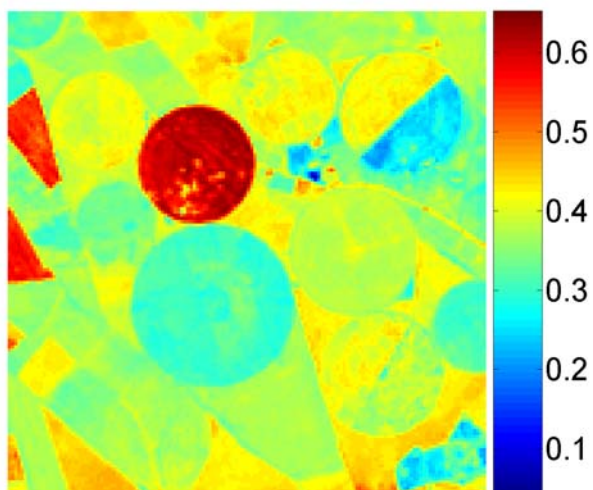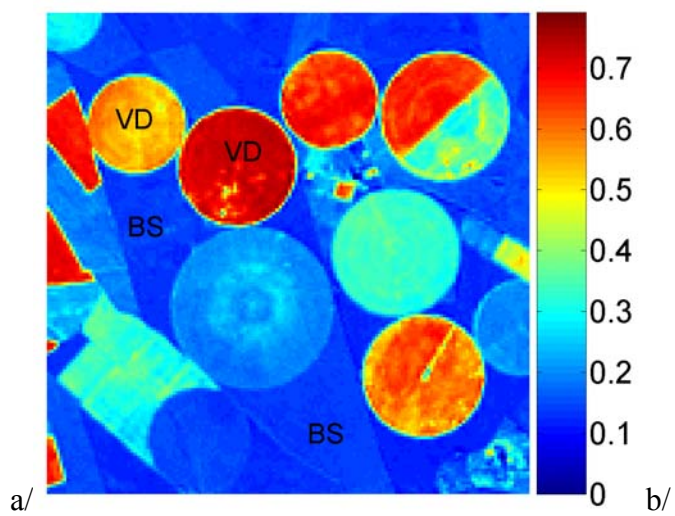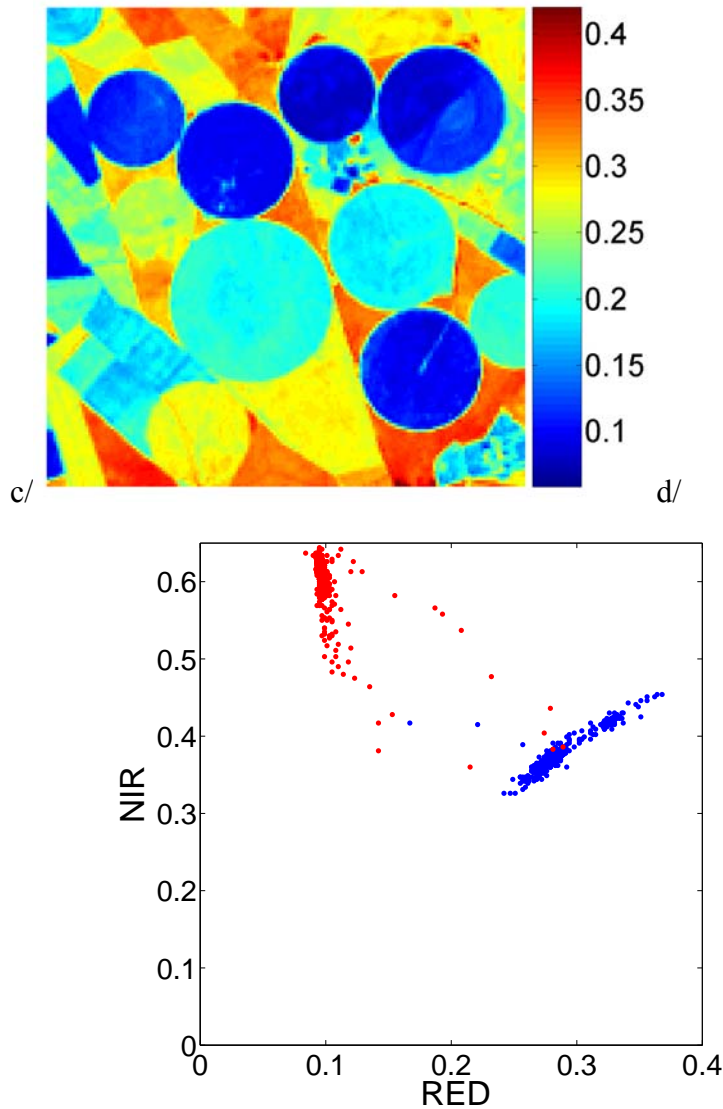
Figure 3: NDVI (a), near infrared (b), red (c) images and near infrared (NIR)/red (RED) plot (d) of Barrax03 (crops). On this site, vegetation discs (VD) are laid over a large bare soil background (BS).The NIR/RED plot is computed over a spatial subset of the scene. The blue points represent bare soil pixels (associated experimental correlation coefficient is $\rho_{exp,bs}$=0.9) and the red points are crop pixels (associated experimental correlation coefficient is $\rho_{exp,crop}$=-0.68)

a/

b/
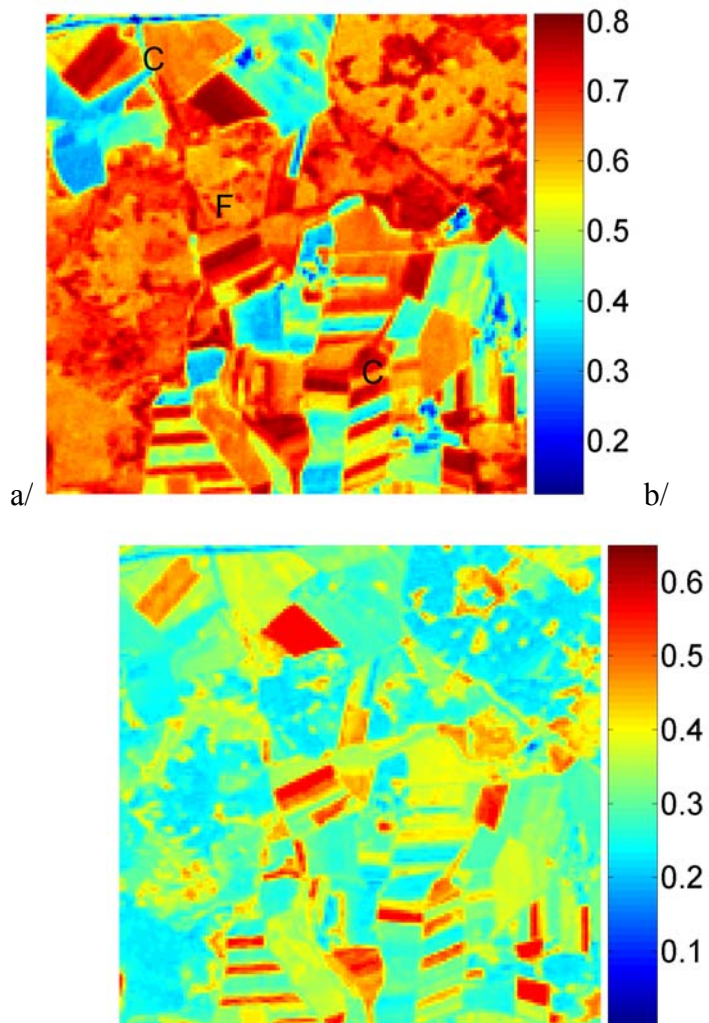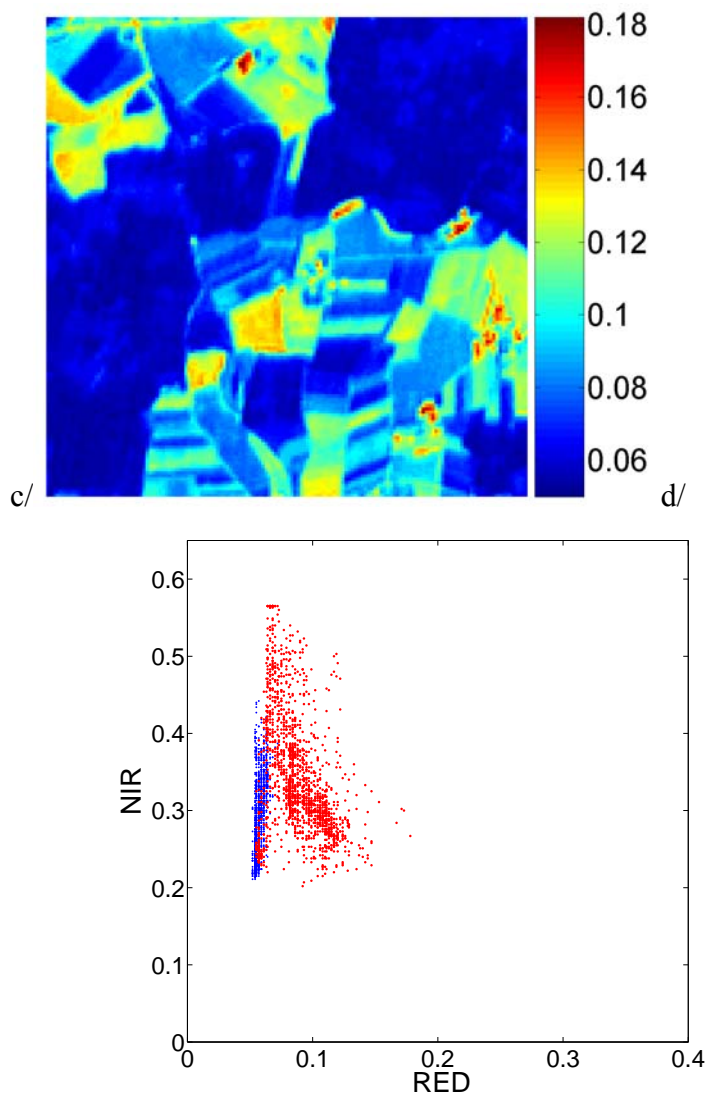
Figure 4: NDVI (a), near infrared (b), red (c) images and near infrared (NIR)/red (RED) plot (d) of Gilching02. This site is composed of a forest area (F) and two crop areas (C). The NIR/RED plot is computed over a spatial subset of the scene. The blue points represent forest pixels (associated experimental correlation coefficient is $\rho_{exp,bs}$=0.6) and the red points are crop pixels (associated experimental correlation coefficient is $\rho_{exp,crop}$=-0.4)
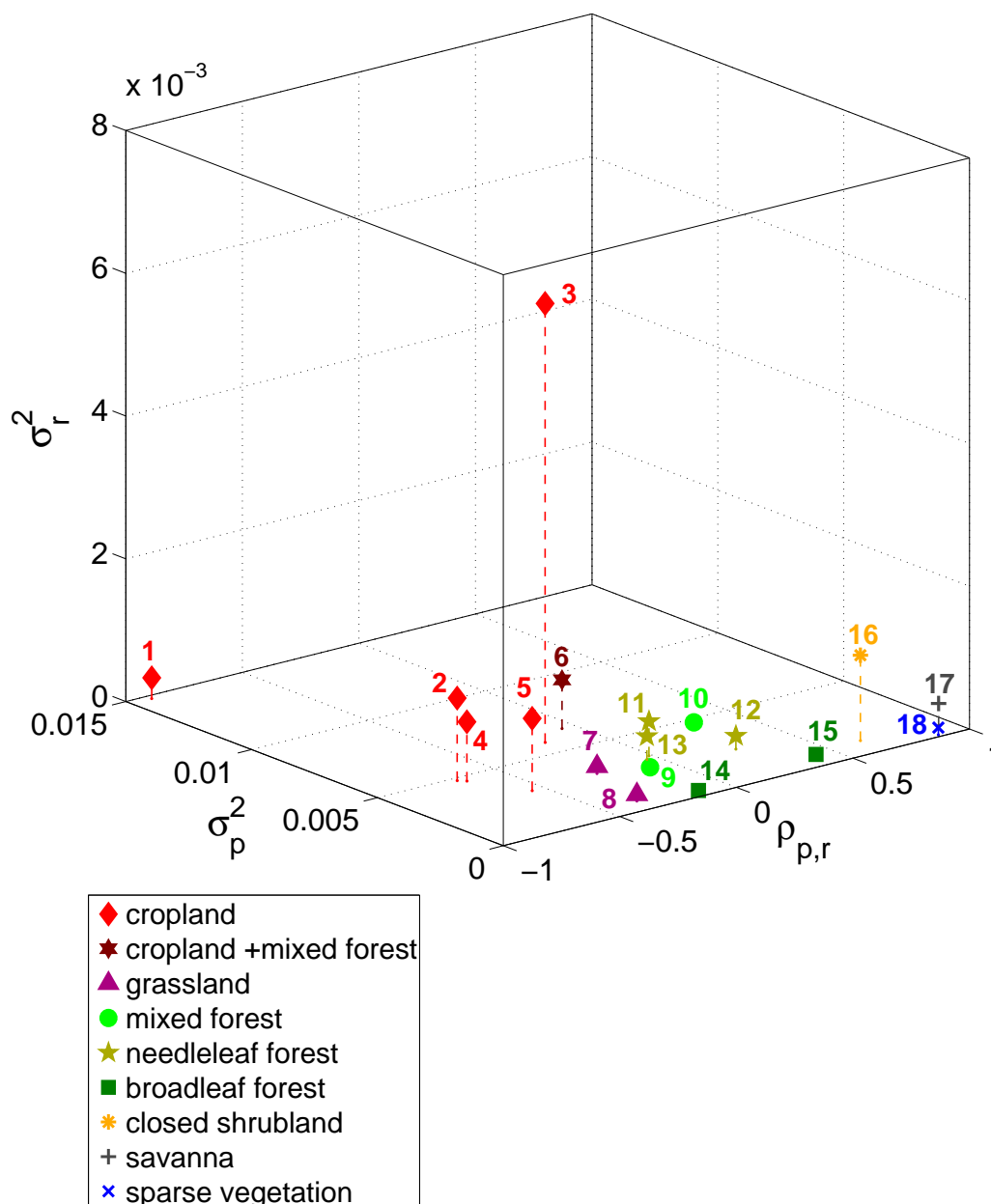
Figure 5 : Parameters (σ_p^2 , σ_r^2, $\rho_{p,r}$) of the linear model of coregionalization applied to the SPOT-HRV scenes under study. The sills σ_p^2 and σ_r^2 quantify the overall spatial variability of near infrared and red reflectances, respectively, over the scene. $\rho_{p,r}$ is an indicator of the overall spatial correlation between red and near infrared reflectances over the scene. The numbers represent the site number given in Table 1.
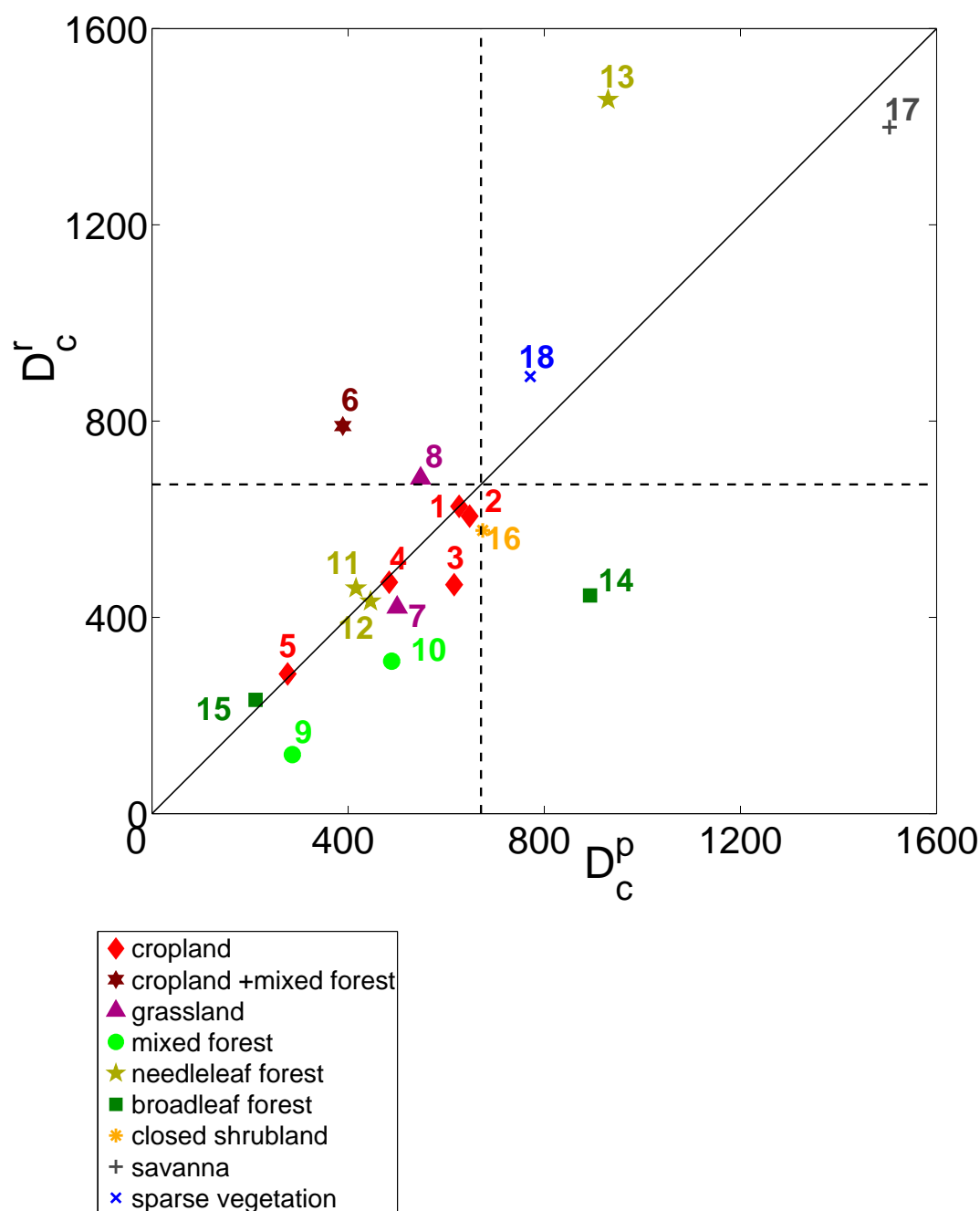
Figure 6: Comparison of the mean extent of the spatial structure captured by red (D_c^r) and near infrared (D_c^p) for the 18 SPOT-HRV scenes under study (numeric values given in Table 3). The numbers represent the site number given in Table 1. The dash lines represent the threshold $D_{c,T,3km}$=671 m above which the image extent of a given variable (red or near infrared) is deemed to be not large enough to encompass the spatial variability of the spatial structures observed in the image and thus the second

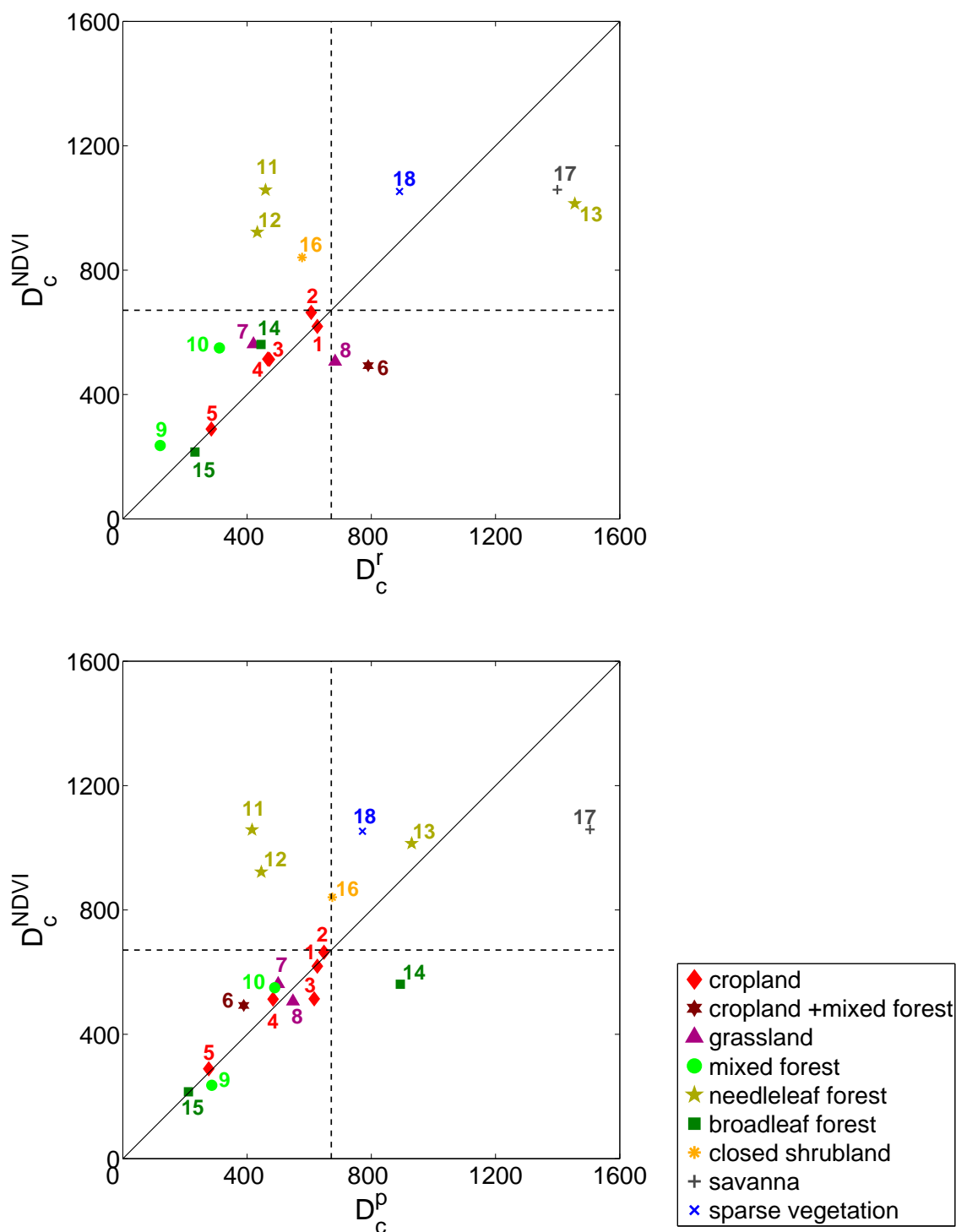order stationarity used to model the variogram of that variable is not consistent with the data.

Figure 7: Comparison of the mean extent of the spatial structure captured by red(D_c^r), near infrared (D_c^p) and NDVI (D_c^{NDVI} provided by Garrigues et al., 2006a) for the 18 SPOT-HRV scenes under study (numeric values given in Table 3). The numbers represent the site number given in Table 1. The dash lines represent the threshold $D_{c,T,3km}$=671 m above which the image extent of a given variable (NDVI, red or near infrared) is deemed to be not large

enough to encompass the spatial variability of the spatial structures observed in the image and thus the second order stationarity used to model the variogram of that variable is not consistent with the data.